Study of the superfluid transition in two-dimensional ⁴He films

D. J. Bishop* and J. D. Reppy

Laboratory of Atomic and Solid State Physics and Materials Science Center,
Cornell University, Ithaca, New York 14853

(Received 21 January 1980)

We have studied the superfluid transition of thin two-dimensional ⁴He films adsorbed on an oscillating substrate. The superfluid mass and dissipation support the Kosterlitz-Thouless picture of the phase transition in a two-dimensional superfluid. In addition we observe finite-velocity effects which are not explained by current dynamic theories. We also report data on two-dimensional ³He-⁴He mixtures.

This paper is a report of our studies of the super-fluid transition in two-dimensional (2D) ⁴He films. Preliminary reports have appeared elsewhere.[1-3] The paper is divided into seven sections. Section I is an introduction. In Sec. II we describe our experiment and discuss our results. Section III discusses the Kosterlitz-Thouless theory and its extension to include dynamic effects by Huberman, Myerson, and Doniach[4] and by Ambegaokar, Halperin, Nelson, and Siggia (AHNS).[5] Section IV discusses the calibration of the oscillator and Sec. V discusses the fits to our data. Section VI presents some preliminary data on ³He-⁴He two-dimensional mixtures and Sec. VII presents our final conclusions. There are three appendices. Appendix A contains the fitting algorithm for the dynamic theory, Appendix B contains the derivation of the constant-temperature theory curve and, Appendix C contains a table summarizing all our data.

I. INTRODUCTION

There has been much work over the years on the question of long-range order in two-dimensional systems. Bloch[6] in 1930 first showed that in one- and two-dimensional magnetic lattices there exists no finite spontaneous magnetization at a nonzero temperature. In 1935 Peierls[7] showed the same for crystalline order and Osborne[8] in 1949 showed that an analogous result holds for momentum order in a Bose gas. Later, more general arguments were put forth concerning long-range order in all two-dimensional systems by Mermin,[9] and Mermin and Wagner.[10] In 1967 Hohenberg[11] showed that the expectation value of the superfluid order parameter in a 2D Bose fluid is zero. Therefore, there appears to be strong theoretical evidence for the fact that super-fluidity of the conventional type should not exist in a two-dimensional system.

However, experimentally there has been much evidence to the contrary. Rollin[12] in 1936 first postulated the existence of the superfluid film to explain an anomalous heat flow into a cryostat. Experimentally saturated films were studied first by Daunt and Mendelssohn[13] in 1939. Superfluid flow in much thinner unsaturated films was first shown by Long and Meyer[14] in 1950 and later by Bowers, Brewer, and Mendelssohn.[15] Since that time an enormous amount of work has been devoted to the study of ever thinner, unsaturated superfluid films.[17] For example recent experiments performed at Cornell[16] have observed the superfluid properties of ⁴He films with a thickness of only 0.01 active atomic layers. Therefore, if the concept of a two-dimensional system has any meaning in an experimental sense then there appears to be a contradiction between theoretical expectation and experimental observation with regard to superfluidity in two dimensions.

There has been much work to reconcile this growing discrepancy between theory and experiment.[17] In 1953 Ziman[18] examined the Bose gas in a slab geometry. He found that in a two-dimensional system of extent L, and thickness D, that the condensation temperature varies as $(\ln L)^{-1}$ as $L \to \infty$. Thus a true two-dimensional Bose system of finite thickness and infinite lateral extent has a transition temperature equal to zero. He speculated that superfluidity in thin films might be due to some finite upper limit on the size of the cooperating superfluid regions of the order of 700 Å. Work was done by Mills,[19] Khorana and Douglass,[20] Goble and Trainor,[21] Dewar and Frankel,[22] and Penrose[23] to further develop this idea.

However, a different approach was taken by other workers. Lasher,[24] Berezinskii,[25] and Kosterlitz and Thouless[26] defined a different type of order to be associated with superfluidity in two dimensions. Long-range order of the conventional sense which was associated with superfluidity in three dimensions is impossible in a two-dimensional system. They defined a new type of order. This new type of order to be associated with superfluidity in two dimensions is referred to as long-range coherence by Lasher and as topological long-range order by Kosterlitz and Thouless. These theories can be applied to the XY model of magnetism, the solid-liquid transition, superconductors, and the neutral superfluid, but not the

Heisenberg ferromagnet.

In the Kosterlitz-Thouless model[26] the two-dimensional superfluid is populated by a system of bound vortex-antivortex pairs. At low temperatures isolated vortices cannot occur because their energy increases logarithmically with the size of the system. However, pairs of vortices with equal and opposite vorticity have finite energy and must occur because of thermal excitation. Such pairs, however, do not destroy the topological long-range order of the system because the net vorticity is zero. At finite temperatures the phase of the order parameter varies with position and the type of long-range order defined by Penrose and Onsager[27] does not exist. However, as long as the order in the system exists locally, the phase can be correlated from region to region. It is this type of order which is associated with the superfluidity in the two-dimensional system.

At higher temperatures a fraction of the pairs dissociate and superfluidity is destroyed. Kosterlitz and Thouless derived the relation between the superfluid density at onset $\rho_s(T_c)$ and the transition temperature T_c. Their result is

$$\frac{\rho_s(T_c^-)}{T_c} = \frac{2}{\pi} k_B \frac{m^2}{\hbar^2} . \tag{1}$$

This equation is the central result of the Kosterlitz-Thouless theory.

Experimentally there has also been much work on this problem. However the results have been more ambiguous than the predictions of the theory. In 1968 there was evidence that the superfluid density in two-dimensional helium films might be nonzero at the superfluid onset. For example third-sound studies by Rudnick's group at UCLA[28] showed that the third-sound signal disappeared while the third-sound velocity was still finite. Also persistent current measurements on helium films[29] indicated that the superfluid critical velocity was becoming zero while the superfluid density was still finite. An attempt was made to explain the anomalous third-sound attenuation seen in the UCLA experiments by applying a macroscopic quantum uncertainty principle to the flow of superfluid helium.[30]

Unfortunately, neither third-sound nor persistent current measurements can be used to pursue the question of the superfluid density behavior in the transition region, since third-sound signals become heavily damped and do not propagate, and persistent currents decay away. The first experiments which were able to examine the superfluid density continuously in the transition region were the quartz microbalance experiments of Chester and Yang.[31] In these experiments, which are similar in concept to the present work, the superfluid density throughout the entire critical region could be measured. Unfortunately these quartz microbalance experiments and

later ones by Herb and Dash[32] failed to measure the dissipation in the system and were performed in the MHz frequency range and showed, as would now be expected on the basis of the dynamic theory, considerable broadening of the transition region. Therefore until recently the experimental situation remained ambiguous. The third-sound results were subject to two interpretations, either at T_c, $\rho_s(T_c)$ was finite, or for $T < T_c$, the dissipation in the system became very large. The quartz microbalance experiments shed no light on the question of a finite ρ_s at T_c because of the broadening of the transition due to the high frequency of the quartz microbalance in accord with the predictions of recent dynamic theories. In addition another vital clue, the peak in superfluid dissipation at the transition, was missed by the experimentalists. They failed to measure *both* the in- and out-of-phase components of their oscillator signals and therefore did not simultaneously measure the superfluid density and dissipation.

In 1975 a modified version of the Andronikashvili[33] method incorporating a high-Q torsional oscillator was used to measure the superfluid density of thin ^{4}He films adsorbed on Vycor glass.[34] At the transition the superfluid density was seen to go continuously to zero characterized by a bulk critical exponent and was not accompanied by any superfluid dissipation. This was interpreted as a result of the three-dimensional character of the substrate with the ^{4}He film behaving as a dilute three-dimensional surface gas.

In 1977 the current ^{4}He film experiments were started using a two-dimensional Mylar substrate in a high-Q Andronikashvili torsional oscillator. At the transition a precipitous superfluid density and a sharp peak in the superfluid dissipation were observed. We were able to follow these features through the transition region with high resolution. We feel that these experiments provided the first unambiguous indication of the precipitous nature of the superfluid density at the critical transition for two-dimensional ^{4}He films. This paper is a discussion of our observations and our analysis of the data through the dynamic theories of Huberman, Myerson, and Doniach[4] and Ambegaokar, Halperin, Nelson, and Siggia.[5]

II. EXPERIMENTAL METHOD

In this section we will describe the Andronikashvili technique used in the present series of experiments. The method due initially to Andronikashvili,[33] has been modified by us for use in our thin-helium-film experiments. The technique makes use of the two-fluid nature of superfluids. In Andronikashvili's original experiment a stack of disks at the end of a torsional fiber was placed in a bath of superfluid helium. The plates are closely spaced such that the normal

fluid is clamped to them and dragged by them as they oscillate. The superfluid component of course is not affected by the plates. By measuring the resonant frequency of the system one can determine the amount of normal mass that is trapped by the plates and determine the superfluid density of the liquid.

Our modification involves using an extremely high-Q torsional oscillator (see for example Refs. 1–3, 16, 34, and 35). By using an oscillator with a $Q \geq 10^5$, we are able to resolve the moment of inertia of the system to better than five parts in 10^9. Thus, even though we have an extremely thin-^{4}He film (a few atomic layers) we have enough resolution to resolve the superfluid mass of these films to one part in 10^4. This technique of course allows us to measure the superfluid mass through the transition region. Other techniques used to investigate superfluid ^{4}He films in a two-dimensional geometry such as third sound, persistent currents, heat transfer, and mobility suffer from loss of signal and/or low precision in the critical region. The quartz microbalance of Chester and Yang[31] does allow one to measure the superfluid mass through the transition region. However, the precision of our experiment is much higher owing to the larger surface area of our cell and the high Q. In addition we measure the dissipation of the superfluid film which provides a crucial piece of information.

In the experiment reported here, helium films are adsorbed on a substrate of Mylar[45] film. The sample cell (shown in Fig. 1) contains a strip of the plastic film 6×10^{-4} cm thick, 1.0 cm wide, and about 21 m

long wound as a spiral on the axis of a torsional oscillator. The helium for the experiment is admitted through the hollow torsion rod. The oscillator is incorporated into a feedback loop consisting of an amplifier, active filter, phase shifter, and zero-crossing detector.[36] In such a circuit the torsional oscillator is the frequency-determining element. Hence by simply counting the resonance frequency of the loop of about 2.5 KHz we can determine the moment of inertia to five parts in 10^9.

In operation, helium is admitted into the cell and the cell is allowed to anneal at a high temperature (~ 10 K). This gives the helium an opportunity to distribute itself uniformly. The cell is then cooled and the period and Q are measured as a function of temperature. At each point the temperature is regulated to ± 10 μK and the period allowed to stabilize to several parts in 10^9 before a reading is taken. Equilibrium time is approximately 30 min. When the oscillator is cooled below the transition temperature, the superfluid decouples from the torsion pendulum and the period of the oscillator decreases (see Fig. 2). In addition, one sees a pronounced narrow peak in the dissipation of the superfluid at the transition (seen in Fig. 2 as a dip in the Q of the system). This dissipation remains at a nonzero level as the temperature is lowered well below the transition temperature. The width of the transition region where the period changes rapidly and the peak in dissipation occurs is less than 1% of the transition temperature.

In practice the quantities in which we are interested are the period shift due to the superfluid and the superfluid dissipation. Shown in Fig. 3 are the shift in period ΔP which is proportional to the superfluid mass and the superfluid dissipation Q^{-1}. The narrowness of the onset features can be seen in this picture.

SIDE VIEW OF EXPERIMENT   SAMPLE CELL ASSEMBLY
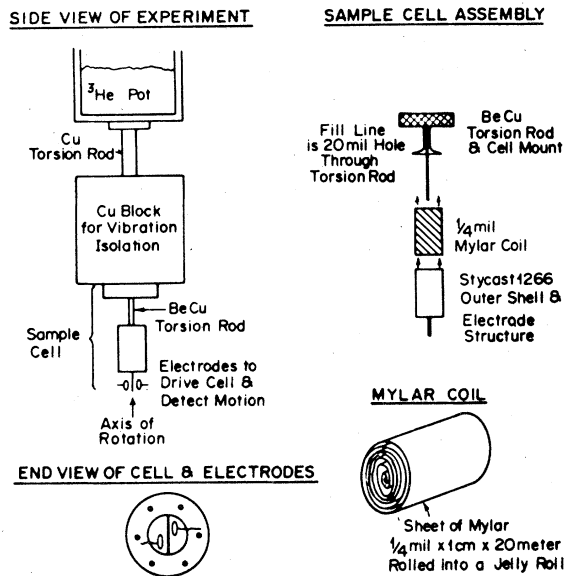

END VIEW OF CELL & ELECTRODES

FIG. 1. Design of the Mylar two-dimensional Andronikashvili cell is shown.
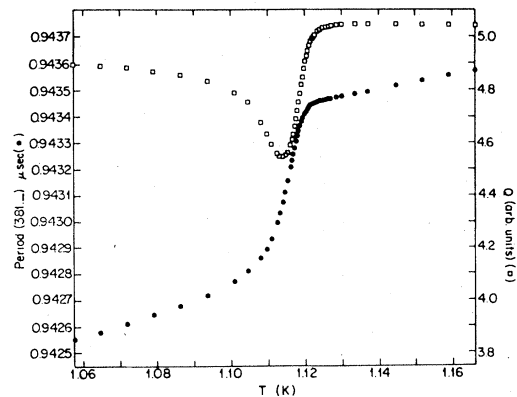

FIG. 2. Period and Q of the Andronikashvili cell are shown as a function of temperature at the superfluid transition.
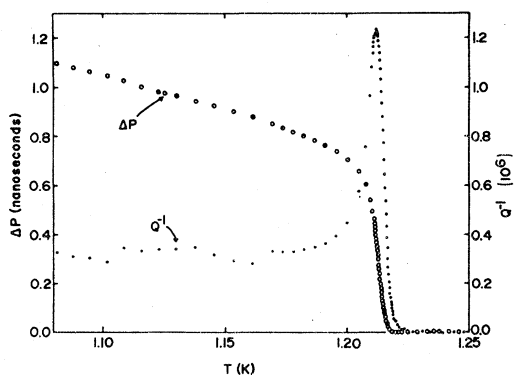
FIG. 3. Shift in period, ΔP, and the change in dissipation attributable to the superfluid, Q^{-1}, are shown as a function of temperature at the superfluid transition.

These features in the dissipation are unique to the two-dimensional superfluid. Neither the Androni-kashvili experiments in bulk helium nor the experiments performed for the films adsorbed on the three-dimensionally connected substrate, porous Vycor glass,[34] exhibit any excess dissipation associated with the superfluid transition. The peak in dissipation in the present experiment points to a fundamental difference between onset phenomena in two- and three-dimensional superfluids.

To further emphasize this difference, shown in Fig. 4 are the superfluid masses as measured by Vycor and 2D Mylar Andronikashvili cells. Note that the Vycor results show a continuous superfluid density at onset. For Vycor the superfluid density (or period shift) obeys a power law of the form

$$\Delta P(T) = A(1 - T/T_c)^\zeta$$

where ζ assumes its bulk value of $\frac{2}{3}$ (see Ref. 34). The Vycor is a three-dimensionally interconnected system and hence the 3D-like behavior of the superfluid density. In contrast however one sees that the
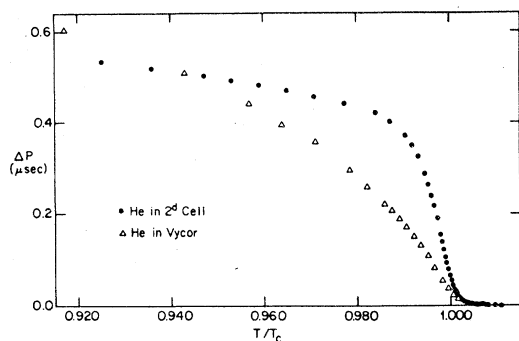
superfluid density in the two-dimensional geometry changes much more sharply at the transition. Therefore both systems have fundamentally different behavior at the transition as regards both the superfluid mass and the dissipation. This emphasizes the crucial role substrate geometry plays in determining the nature of the superfluid transition in thin ^{4}He films.

In practice the dissipation peak shown in Fig. 3 (and to a lesser extent the period shift) are dependent on the velocity of the cell as is shown in Fig. 5. We show the dissipation peak for the same thickness film for three different drive velocities. As the drive velocity is increased, the dissipation peaks broaden out, become larger, and move to lower temperatures. At low velocities (less than 10^{-3} cm/sec) we find that the period and Q^{-1} are velocity independent, while at larger velocities nonlinear effects set in, and the transition region and dissipation peak are broadened. This is shown in Fig. 6. We have plotted for a single film thickness the width of the dissipation peak as a function of cavity velocity. Note that for velocities less than 10 μm/sec, the width is independent of velocity. However as the cell velocity is increased beyond some critical value the height and width become a function of velocity.

The dynamic extension of the Kosterlitz-Thouless theory described in Appendix A is inappropriate to model the data in the high-velocity regime. The version of the theory by AHNS[5] worked out in Appendix A assumes the validity of linear response. Unfortunately this assumption is no longer valid in the high-velocity regime. Therefore the fits to theory can only be made using the low-velocity data. As we understand it, work on a more complicated version of the theory allowing for high-velocity effects is

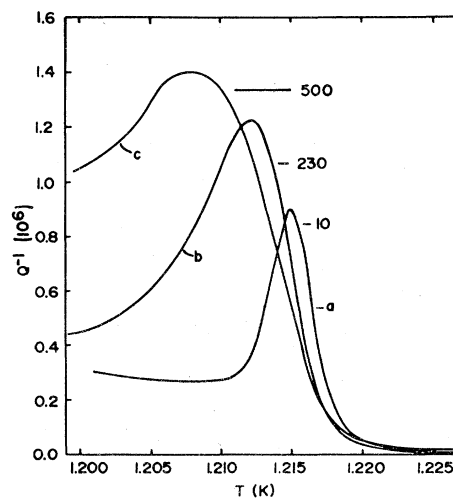FIG. 4. Superfluid period shift for ^{4}He in a Vycor and Mylar Andronikashvili cell.

FIG. 5. Dissipation peak for a single film at three different values of cavity velocity (arbitrary units).
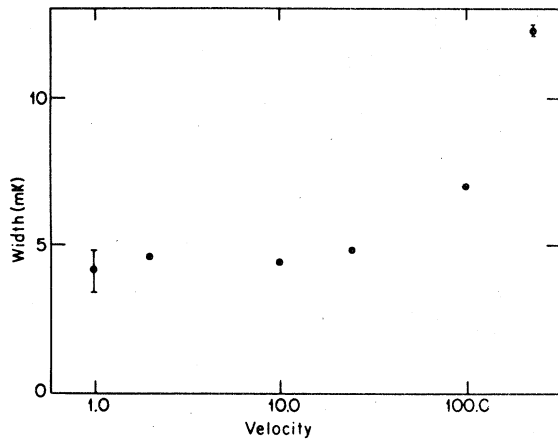
FIG. 6. Width of the dissipation peak as a function of cavity velocity (in arbitrary units).

currently underway.[37]

In Fig. 7 we display the thickness dependence of the transition temperature T_c for the two-dimensional superfluid. Note that we observe a very good linear dependence. The nature of the cell design is such that it has a large open volume (1.2 cm^3). This requires that at higher temperatures allowance be made for gas admitted into the cell which remains vapor, not absorbed onto the Mylar substrate. The three
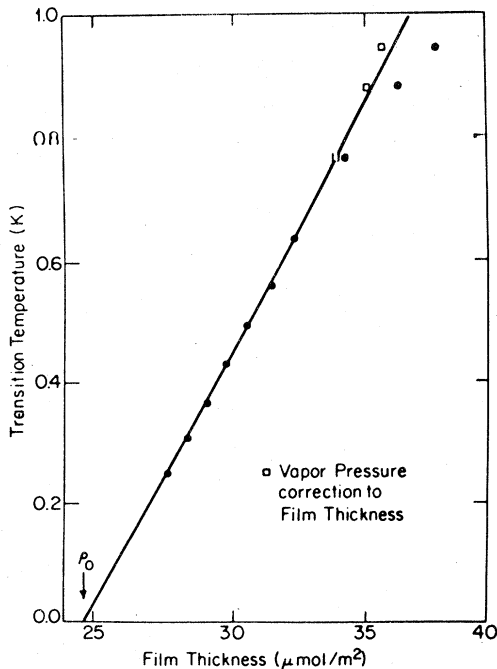

FIG. 7. Transition temperature as a function of film thickness. The open squares have been corrected for the vapor pressure of the ^{4}He gas in the cell. The intercept ρ_0 is 24.91 μmol/m^2.

highest points in Fig. 7 have been so corrected.

In Sec. III we discuss the Kosterlitz-Thouless static theory and its extension to include dynamic effects by Ambegaokar, Halperin, Nelson, and Siggia and by Huberman, Myerson, and Doniach.

III. KOSTERLITZ-THOULESS THEORY

In the Kosterlitz-Thouless model,[26] which we wish to use to interpret our measurements, the two-dimensional superfluid is populated by a system of bound vortex-antivortex pairs. At low temperatures isolated vortices cannot occur because their energy increases logarithmically with the size of the system. However, pairs of vortices with equal and opposite vorticity have finite energy and must occur because of thermal excitation. Such pairs, however, do not destroy the topological long-range order of the system because the net vorticity is zero. At finite temperatures the phase of the order parameter varies with position and the type of long-range order defined by Penrose and Onsager[27] does not exist. However, as long as the order in the system exists locally, the phase can be correlated from region to region. It is this type of order which is associated with the superfluidity in the two-dimensional system.

At higher temperatures a fraction of the pairs dissociate and superfluidity is destroyed. In a simple argument Kosterlitz and Thouless derived the relation between the superfluid density at onset $\rho_s(T_c)$ and the transition temperature T_c. Their argument goes as follows:

The energy and entropy of a single vortex both depend logarithmically on the size of the system. The energy term will dominate the free energy at low temperatures and the probability for the appearance of a single vortex will be very small. However, at some point the entropy term will dominate the free energy and vortices will appear spontaneously. The critical temperature is given by the point at which the free energy changes sign.

An isolated vortex has a velocity field given by ($n = 1$)

$$\vec{V}_s(r) = \frac{\hbar}{m}\hat{Z} \times \vec{\nabla} \ln\left[\frac{R}{a}\right] , \tag{2}$$

where a is the size of the vortex core, R is the size of the system, and $\hat{Z}$ is normal to the surface. The energy of such a vortex is given by

$$E = \frac{1}{2}\rho_s \int_a^R d^2r \ V_s^2 = \rho_s \frac{\hbar^2}{m^2}\pi \ln\left[\frac{R}{a}\right] . \tag{3}$$

The entropy of a free vortex is given by

$$S = k_B \ln\left[\frac{R^2}{a^2}\right] . \tag{4}$$

We set the free energy $(E - T_c S)$ equal to zero and obtain the final result

$$\rho_s(T_c^-) = \frac{2}{\pi} k_B \frac{m^2}{\hbar^2} T_c \ . \tag{5}$$

This is the central result of the entire Kosterlitz-Thouless static theory. This result was derived in their original paper (see Ref. 26) as a result of a more sophisticated calculation.

In a subsequent publication Kosterlitz[38] rederived this result in a renormalization-group calculation. He also first pointed out that Eq. (5) implies that the superfluid mass is *nonzero* at onset. This was verified by another renormalization-group calculation by Jose, Kadanoff, Kirkpatrick, and Nelson.[39] Further, as has been emphasized by Nelson and Kosterlitz,[40] Eq. (5) implies that the ratio of the superfluid mass per unit area at onset to the transition temperature, is a *universal* quantity, independent of film thickness. It is this central prediction of the Kosterlitz-Thouless theory which we will address in our discussion of the experimental results.

In the Kosterlitz-Thouless static theory the superfluid density near the transition is given by (see, for example, Ref. 40)

$$\rho_s(T) = \rho_s(T_c^-)[1 + b(1 - T/T_c)^{1/2}] \ . \tag{6}$$

In this formula, the superfluid density at onset $\rho_s(T_c^-)$ is given by Eq. (5). The square-root cusp at the transition is due to interactions among vortices which were ignored in the original calculation of Kosterlitz and Thouless[26] but which were later taken into account in a calculation by Kosterlitz.[38] The quantity b determines the strength of the square-root cusp in Eq. (6). As the result of a mean-field calculation, Nelson and Kosterlitz[40] estimate b to be of the order of 0.5. However, its value is expected to be *nonuniversal*. Shown in Fig. 8 is the prediction of the static theory for the superfluid density for various thickness films using the results of Ref. 40.
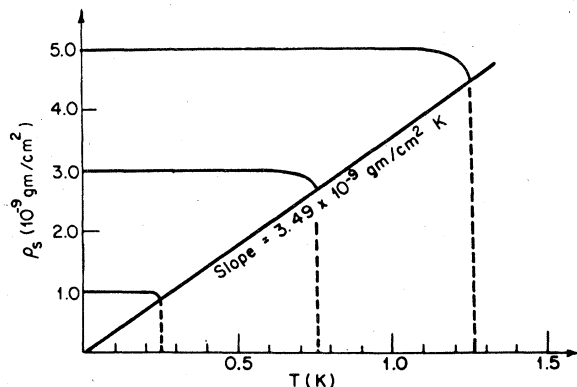

FIG. 8. This figure shows the superfluid density for three different thickness films as a function of temperature according to the Kosterlitz-Thouless static theory.

Unfortunately, present techniques for the determination of the superfluid mass in thin-helium films cannot test the static theory directly, since they all require measurements at a nonzero frequency and superfluid velocity. As a result, one does not expect to see the discontinuous jump in the superfluid mass in the static theory, but to find a continuous variation with temperature at the transition. In addition, one expects to find considerable dissipation associated with the vortex motion induced by the superflow required for the superfluid mass measurements.

The problem of dissipation at the phase transition in a two-dimensional superfluid has been treated recently by Huberman, Myerson, and Doniach[4] and Ambegaokar, Halperin, Nelson, and Siggia (AHNS).[5] These authors have extended the static Kosterlitz-Thouless theory to the case of finite frequency and nonzero superfluid velocity.

The behavior of the two-dimensional superfluid as seen in our experiment can be understood in terms of the dynamic theory of Ambegaokar, Halperin, Nelson, and Siggia[5] (AHNS). In their theory, as well as in the calculation of Huberman, Myerson, and Doniach[4] dissipation is associated with the diffusive motion of two-dimensional vortices driven by the oscillating superflow. The more comprehensive form of the dynamic theory given by AHNS[5] is directly applicable to the data in the high-frequency regime where the present experiment is performed. The theory of Huberman *et al.* is valid in the limit of zero frequency and finite amplitude while the theory of AHNS is valid for finite frequencies and small amplitudes. Because our experiments were performed at finite frequencies it is the theory of AHNS that we have used in our analysis.

In the analysis performed by AHNS the dissipation of energy is due to the diffusive motion of free vortices and the polarization of bound pairs. Contributions from free vortices and bound pairs enter in the various regimes. Using the results of their theory they have derived the observed period shift and dissipation for a ^{4}He film adsorbed on an oscillating substrate. The details of the derivation are given in Appendix A.

In brief, the reduced period shift $2\Delta P/P$ and the superfluid dissipation Q^{-1} are related to a frequency-dependent dielectric constant ϵ by the following relations:

$$\frac{2\Delta P}{P} = \left[\frac{A}{M}\right] \rho_s(T_c^-) \, \text{Re}(\epsilon^{-1}) \ , \tag{7}$$

$$Q^{-1} = \left[\frac{A}{M}\right] \rho_s(T_c^-) \, \text{Im}(-\epsilon^{-1}) \ . \tag{8}$$

The real part of ϵ is taken as due to bound pairs according to Eq. (9a) of AHNS. It is calculated by a numerical integration of the Kosterlitz recursion rela-

tions (see Appendix A for details). For the ima-
ginary part of ϵ contributions due to bound pairs,
free vortices, and a constant background (to account
for the dissipation remaining well below the transi-
tion) are added together. The static theory contains
three parameters $\rho_s(T_c^-)$, T_c, and b. The dynamic
theory contains three more parameters in addition to
those in the static theory. There is a dimensionless
parameter $\ln(2D/\omega a^2)$ related to the vortex diffusion
constant D, the vortex core radius a, and the fre-
quency of the oscillator ω. There is a coefficient of
the free-vortex dissipation and a background term,
mentioned above, which plays almost no role in the
transition region.

In Eqs. (7) and (8), the term (A/M) is the ratio
of the area of the Mylar substrate A to the effective
mass M of the pendulum bob when the pendulum is
treated as a linear oscillator. The ratio is obtained
from a knowledge of the area of the substrate and a
measurement of the sensitivity of the oscillator
period to changes in the mass per unit area of the ad-
sorbed helium. This calibration is described in Sec.
IV.

In the analysis of our data taken for different cov-
erages of adsorbed helium, we allow the value of the
Kosterlitz-Thouless jump $\rho_s(T_c^-)$ to be a free param-
eter to be determined by an optimization of the fit of
relations (7) and (8) to the data. This is later
described in more detail.

IV. OSCILLATOR CALIBRATION

To fit our data to Eqs. (7) and (8) we need to mea-
sure the quantity (A/M) for our system, where A is
the area of the substrate and M is its effective mass.
The area is taken to be the geometric surface area of
the Mylar film which is 0.428 m^2. The effective mass
of the pendulum bob is obtained by treating the sys-
tem as a linear harmonic oscillator.

The measurement of the oscillator effective mass
or the calibration of the sensitivity of the oscillator
period to changes in the mass per unit area of the ab-
sorbed helium is obtained from a separate experi-
ment. For the calibration measurement, we hold the
temperature of the system constant and observe the
period of the oscillator as the mass per unit area of
adsorbed helium is increased (this is shown in Fig.
9). When the coverage of helium is less than a criti-
cal amount, which depends on the temperature at
which the observations are made, the adsorbed heli-
um is entirely locked to substrate and contributes its
entire moment of inertia to the pendulum bob. By
measuring the amount of helium adsorbed on the
substrate we determine the sensitivity of the period
to the adsorbed mass per unit area at a nonzero fre-
quency and superfluid velocity. The slope $(\Delta P/\Delta \rho)$
of the line in this region where normal fluid is being

added to the system is related to the effective mass
M of the oscillator by

$$M = \tau / 2 \left| \frac{\Delta P}{\Delta \rho} \right| = 5.09 \text{ g} ,$$

where τ is the period. This effective mass is used in
conjunction with the area to calculate the prefactors
of Eqs. (7) and (8).

When the film coverage is increased above a criti-
cal amount, superflow becomes possible and a nearly
discontinuous drop in the period of the oscillator is
observed (see Fig. 9). Of course the variation of
period with coverage is actually continuous, but to
trace out the continuous variation, as is done in the
temperature sweeps (see Figs. 2 and 3), would be
very tedious, since steps of 10^{-3} of total coverage
would be required.

The solid line in Fig. 9 is a theory curve using the
static-theory formula given in Eq. (6). As previously
pointed out this sort of measurement represents a
fairly low resolution picture of what is happening at
the transition. The difference between the static and
dynamic theory when viewed in a picture such as Fig.
9 represents a difference about equal to the size of
the dots in the picture. Therefore we can safely
make use of the static theory to analyze this particu-
lar measurement.

Starting with the static-theory formula, Eq. (6), we
obtain the following formula for the period during a
constant temperature measurement (see Appendix B
for details). The jump occurs at density ρ_1, and tem-
perature T_1. ρ is the total density.

For $\rho < \rho_1$

$$\tau = \left| \frac{\Delta P}{\Delta \rho} \right| \rho + P_0 ,$$ (9)

where $(\Delta P/\Delta \rho)$ is the slope of the normal-fluid re-
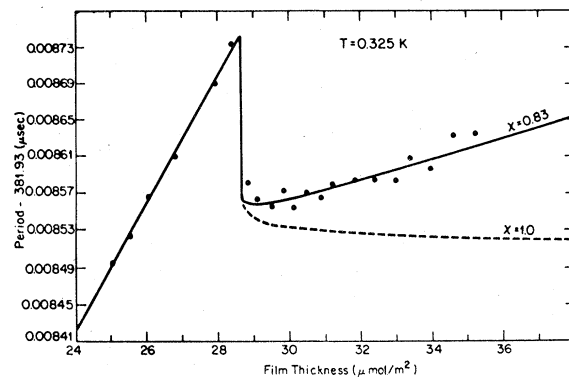

FIG. 9. Period as a function of film thickness at a con-
stant temperature. The solid and dashed lines are the
results of the static theory for two different values of X, the
roughness factor.

gion of Fig. 9 and P_0 is the intercept and ρ is the total density.

For $\rho \geq \rho_1$

$$\tau = \left| \frac{\Delta P}{\Delta \rho} \right| \left| \rho - (1-\chi)AC(\rho-\rho_0) \right.$$

$$\times \left\{ 1 + \left[\left(\frac{1}{AC} \right) - 1 \right] \left(\frac{p-p_1}{p-p_0} \right)^{1/2} \right\} \right| + P_0 \quad , \quad (10)$$

where A is the slope of the transition temperature versus density line and ρ_0 is the intercept. C is the value of the Kosterlitz-Thouless jump and χ is the fraction of superfluid coupled to the surface.

In our formula χ is the only adjustable parameter. $(1-\chi)$ represents the fraction of superfluid inertia which decouples from the oscillator. Shown in Fig. 9 are the formulas (9) and (10) for two different values of χ. By fitting our data in an experiment such as this we can measure the roughness of the Mylar surface. For example, a good fit is obtained in Fig. 9 with $\chi = 0.17$. Also shown in the figure is the theory for a $\chi = 0.0$. This case would correspond to a perfect Andronikashvili experiment in which all of the superfluid decouples from the surface. Presumably this inertial coupling of the superfluid in our experiment is due to wrinkles and other imperfections on our Mylar substrate.

In Sec. V we discuss the fits of our data to the Kosterlitz-Thouless theory using the dynamic extensions of AHNS. The value of the Kosterlitz-Thouless jump $\rho_s(T_c^-)$ is determined and compared with previous third-sound values.

V. FITS TO THE DATA

In this section we discuss the fits to the data using the dynamic extension of the Kosterlitz-Thouless static theory due to AHNS. In the first part of this section we discuss fits to the period shift using a linearized version of the Kosterlitz relations. In the second part we discuss a fit to the dissipation using a numerical integration of the Kosterlitz recursion relations. Derivations of all formulas used in this part are given in Appendix A.

In the low-velocity regime AHNS obtain the following relations for the reduced period shift Eq. (7) and superfluid dissipation Eq. (8), where

$\epsilon = \epsilon' + i(\epsilon'' + \epsilon_b'')$.

In the linear approximation (see Appendix A):

$$\epsilon' = \left\{ 1 + x \coth \left[x \ln \left(\frac{14D}{a^2\omega} \right) \right] \right\}^{-1} \quad , \quad (11)$$

$$\epsilon'' = \frac{1}{2}\pi(\epsilon'x)^2 \left\{ \sinh \left[x \ln \left(\frac{14D}{a^2\omega} \right) \right] \right\}^{-2} \quad , \quad (12)$$

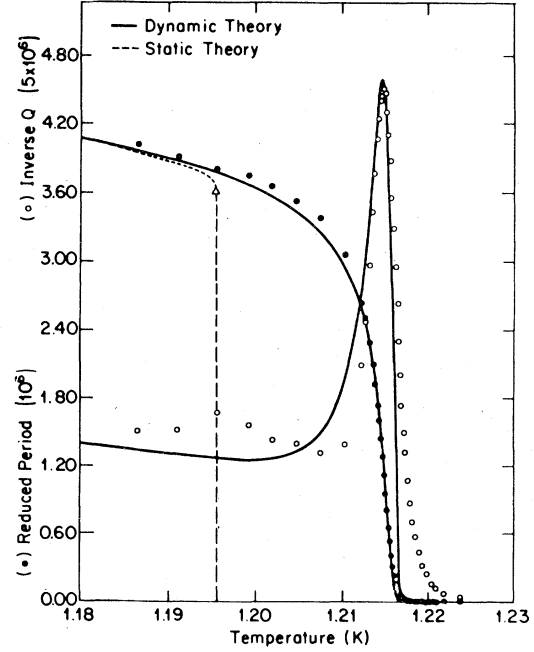where $x = b(|1 - T/T_c|)^{1/2}$, b is the strength of

FIG. 10. Reduced period shift, $2\Delta P/P$, and dissipation Q^{-1} are shown for a superfluid transition of 1.215 K. The solid lines are fits using the linearized version of the dynamic theory of AHNS. The dashed curve is the result of the static theory.

square-root cusp [see Eq. (6)], $\ln(14D/a^2\omega)$ is the dynamic parameter, and ϵ_b'' is the vortex friction coefficient to account for dissipation remaining well below transition. When $T > T_c$, sin and cot appear instead of sinh and coth.

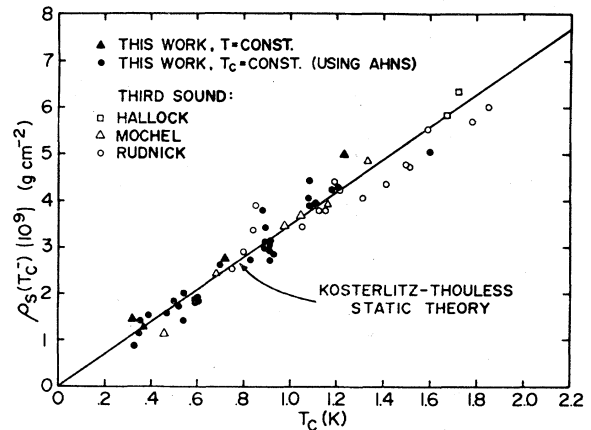We have used this linear approximation to fit the

FIG. 11. Results of all our data, in addition to previous third-sound results for the discontinuous superfluid density jump $\rho_s(T_c^-)$ as a function of temperature. The solid line is the Kosterlitz-Thouless static theory.

period shifts measured in our experiment. Using formula (7) in a nonlinear-least-squares fitting routine[41] we have obtained values of $\rho_s(T_c^-)$, b, and T_c for our films. An example of such a fit is shown in Fig. 10. The linear approximation is not expected to be valid near the region where ΔP goes to zero. Therefore the fit to the dissipation peak must be viewed as fortuitous. However, for temperatures lower than that temperature the linearized theory is valid, and we may use it to fit the $2\Delta P/P$ data to obtain values for the static parameters b, T_c, and $\rho_s(T_c^-)$ in the theory.

Shown in Fig. 11 are the most significant results of our experiment. We have plotted in that figure the values of $\rho_s(T_c^-)$ obtained from our fits for our data. Also plotted in that figure are the values of the Kosterlitz-Thouless jumps obtained from experiments at constant temperature (see for example Fig. 9).

The older third-sound experiments can also be analyzed in terms of our present understanding to obtain estimates of the Kosterlitz-Thouless jump in the superfluid mass per unit area at the two-dimensional phase transition. Although it is not possible to follow a third-sound signal right through the transition region, it can be followed to the point where the dissipation begins to rise rapidly. If the third-sound signal disappears at this point, then as can be seen in Fig. 3 the value of the superfluid mass is still up on the shoulder of the curve and a reasonably good estimate for the static value of the Kosterlitz-Thouless jump can be obtained. Recently, Rudnick[42] has reanalyzed his third-sound data using his latest estimate of the van der Waal's constant, and has obtained values for $\rho_s(T_c^-)$ which are in good agreement with the value predicted by the Kosterlitz-Thouless theory.[26,38]

In Fig. 11 we have plotted as a function of the transition temperature, the values for the static jump in the superfluid density obtained from the two analyses of our data using the dynamic and static theory. We have also included in Fig. 11 the estimates obtained by Rudnick[42] and additional values provided by Mochel[43] and Hallock[43] from their third-sound work. The solid line drawn in the figure is the theoretical prediction given by Kosterlitz and Thouless. As is clear, the data from all the different experiments are in good general agreement with the theoretical prediction and therefore provide strong support for the Kosterlitz-Thouless picture of the phase transition in the two-dimensional superfluid.

Roth, Jelatis, and Maynard[44] have also published measurements of the third-sound velocity and superfluid onset of ^{4}He films adsorbed on Grafoil. The values they obtain for the universal jump $\rho_s(T_c^-)/T_c$ are in agreement with the experimental results presented here and with theoretical expectations. Their data provide further evidence for the universal nature of the superfluid onset in two dimensions.
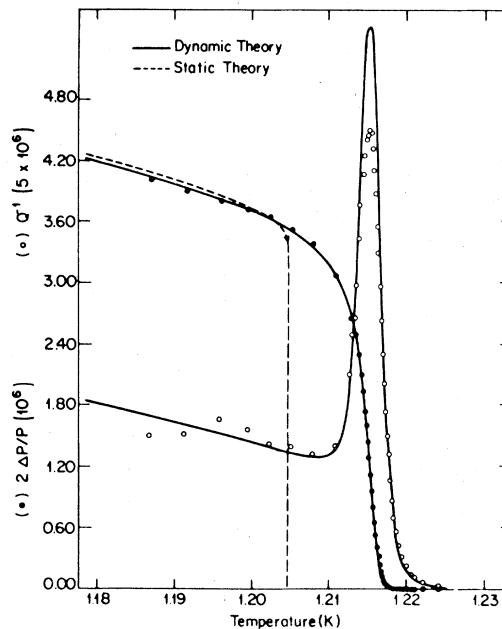
As was pointed out by Nelson and Kosterlitz[40] a

FIG. 12. Reduced period shift, $2\Delta P/P$, and dissipation Q^{-1} are shown for a superfluid transition of 1.215 K. The solid lines are the fits using the dynamic theory of AHNS using the full Kosterlitz recursion relations. The dashed curve is the result of the static theory.

measurement of the quantity $\rho_s(T_c^-)$ also represents a measure of the two-dimensional exponent η. They find that

$$\eta(T_c) = \frac{m^2 k_B T_c}{2\pi\hbar^2 \rho_s(T_c)} \quad . \tag{13}$$

We measure $\rho_s(T_c^-)/T_c$ to be 3.5×10^{-9} g/cm^2 K $\pm 15\%$. Therefore we have experimentally determined η to be

$$\eta = 0.25 \pm 15\% \quad . \tag{14}$$

Finally we would like to discuss a fit performed using the full integrated Kosterlitz recursion relations. Teitel et al. have performed a fit of the data using relations (7) and (8), but without the linearized dielectric constants in Eqs. (11) and (12). This is described in detail in Appendix A. The results are shown in Fig. 12. Unlike the linearized version, these relations should be valid throughout the entire critical region. Note the very good fit to the entire curve. As before, the dashed line in Fig. 12 represents the static predictions. The discrepancy between the solid and dashed lines indicates the magnitude of the dynamic effects observed in our experiments.

VI. ^{3}He-^{4}He MIXTURES

In this section we would like to show some preliminary results on ^{3}He-^{4}He mixtures in the two-dimensional Mylar[45] cell. Shown in Fig. 13 are the superfluid period shift and dissipation for a pure ^{4}He film (lower graph) and for the same film with 10 at.% ^{3}He added (upper graph).

The pure ^{4}He film had a thickness of 36.5 μmol/m^2. Several features should be noted. For all ^{4}He films studied there were observed third-sound standing waves in the superfluid dissipation below T_c. These correspond to numerous third-sound modes which coincided with the oscillator frequency as the temperature was changed. These third-sound resonances can be seen as apparent scatter in the superfluid dissipation data below T_c. However the instrumental scatter in the data is quite small (less than the

width of the dots in Fig. 13) as can be seen by the data above T_c. Therefore these resonances are an indicator of the superfluid nature of the system we are studying. In the pure film shown in Fig. 13 we see the third-sound resonances in the dissipation below T_c, the dissipation peak at T_c and a quiet dissipation signal above T_c. The period shift drops precipitously at T_c. The bulk of this paper is devoted to a discussion of these features. This film had a T_c of 0.91 K.

However the addition of 10 at.% ^{3}He to this film produces several startling effects. These are shown in the upper graph in Fig. 13. The single superfluid transition in the pure film which was accompanied by a precipitous change in superfluid mass and a sharp dissipation peak was replaced by two transitions in the ^{3}He-^{4}He film. We call the pure transition type A. In the pure-film transition type A occurs at 0.91 K. However in the mixture film transition type A is lowered to 0.80 K and is replaced by a second transition (at a slightly higher temperature) which we call type B. Therefore in the ^{3}He-^{4}He film we see evidence of *two* superfluid transitions. The first type A is the conventional Kosterlitz-Thouless transition with a sharply dropping superfluid mass and a dissipation peak. The distinctly different type of transition type B has a continuously and slowly changing superfluid mass at onset and no dissipation peak. The presence of third-sound resonances indicates that both regions below A and between A and B are superfluid. The film was heated and cooled several times and the features always reproduced. Therefore we conclude from these preliminary results that we have seen evidence for *two* superfluid phases in two-dimensional mixtures.

In recent quartz-microbalance studies by Webster, et al.[46] the Kosterlitz-Thouless jump for ^{3}He-^{4}He mixtures was measured. Up to concentrations of 30 at.% ^{3}He they measured no change in the value of the Kosterlitz-Thouless jump. Our data qualitatively supports this result. The height of the shoulder of the superfluid mass curve in our data which is a measure of the Kosterlitz-Thouless jump does not change upon the addition of ^{3}He. Therefore we support their conclusion that the Kosterlitz-Thouless jump is universal under the addition of ^{3}He. However, the quartz microbalance experiment by Webster et al. has less resolution of the superfluid mass and does not measure the superfluid dissipation at all. Therefore it is possible that they have missed these effects which we have observed.

In conclusion we stress that these are preliminary results but they do show some interesting features which, if borne out by further experiment, will bear on such questions as two-dimensional phase separation. In any event these results point out the richness of films of mixtures of ^{3}He-^{4}He as an experimental system for studying various ideas of two-dimensional physics.
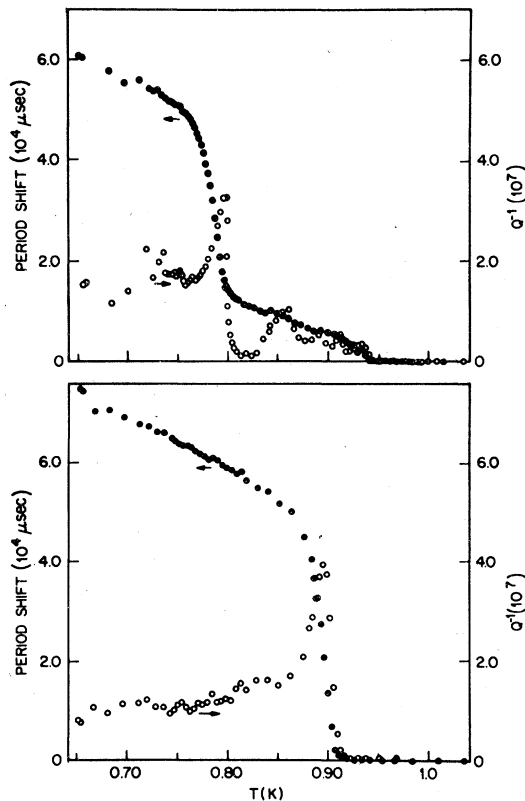
FIG. 13. This figure shows the superfluid period shift and superfluid dissipation for a pure ^{4}He film (lower graph) and for the same film with 10 at.% ^{3}He added (upper graph). Note the presence of third-sound resonances (which can be seen only in a superfluid) below T_c in the pure film and in both lower-temperature phases in the mixture film. These resonances indicate the superfluid nature of the two low-temperature phases in the mixture data.

VII. CONCLUSIONS

In conclusion we have measured the superfluid density and dissipation of a thin two-dimensional helium film at its superfluid transition. We observe a peak in the superfluid dissipation and a sharply changing superfluid density which, when analyzed in terms of the dynamic theory of Ambegaokar, Halperin, Nelson, and Siggia support the Kosterlitz-Thouless picture of the phase transition in a two-dimensional superfluid. The value for the jump in the superfluid density at the transition given by Kosterlitz and Thouless as $\rho_s(T_c^-) = 8\pi k_B(m/h)^2 T_c$, is in good agreement with measured values from experiment. We have observed finite velocity effects in our experiment. The dynamic theories of Refs. 4 and 5 seem capable of describing the data in the low-velocity regime.

ACKNOWLEDGMENTS

APPENDIX A

In order to relate the measured dissipation and period-shift curves to the theory proposed by AHNS, we first summarize the main results of that theory.

For a helium film being driven by a small oscillating external velocity of strength $\vec{v}_n$ and frequency ω, we relate the average superfluid velocity $\vec{u}_s(t)$ to $\vec{v}_n$ by defining a dynamic dielectric constant $\epsilon(\omega)$ as follows:

$$\frac{v_n}{\epsilon(\omega)} = v_n - u_s \quad . \tag{A1}$$

This dielectric constant $\epsilon(\omega)$ is composed of two parts: a contribution due to the motion of free vortices, and a contribution due to the motion of bound vortex pairs. We denote these pieces as ϵ_f and ϵ_b, respectively. The additive contribution due to free vortices has the form [AHNS Eq. (7)]

$$\epsilon_f = \frac{iDh^2\rho_0}{\omega m^2 k_B T} n_f \quad , \tag{A2}$$

where D is the diffusion constant of vortices, m is the mass of the helium atom, ρ_0 is the unrenormalized superfluid density, and n_f is the density of free vortices.

Furthermore,[5,47]

$$\epsilon_b = \bar{\epsilon}(\sqrt{14D/\omega}) + i(\tfrac{1}{4}\pi)\left[r\frac{d\bar{\epsilon}}{dr}\right]_{r=\sqrt{14D/\omega}} \quad , \tag{A3}$$

where $\bar{\epsilon}(r)$ is the static length-dependent dielectric constant.

We now show how the dissipation Q^{-1} and period shift $2\Delta P/P$ are related to this $\epsilon(\omega)$. The time averaged power dissipated per unit area is given in AHNS Eq. (6) as $\tfrac{1}{2}\rho_0 v_n^2 \omega \operatorname{Im}[-\epsilon^{-1}(\omega)]$.

Since the energy stored is $\tfrac{1}{2}Mv_n^2$, where M is the total mass of the system, and the period of oscillations is $2\pi/\omega$, we have

$$Q^{-1} = \frac{1}{2\pi}\frac{\mathcal{P}}{E} = \frac{\rho_0 A}{M}\operatorname{Im}[-\epsilon^{-1}(\omega)] \quad , \tag{A4}$$

where A is the surface area of the substrate, $\mathcal{P}$ is the power dissipated per cycle, and E is the energy stored.

The period shift is determined by considering the force on the substrate due to the motion of the helium film. The momentum density of the film is

$$\vec{g} = \rho_0\vec{u}_s + (\rho - \rho_0)\vec{v}_n = [\rho - \rho_0/\epsilon(\omega)]\vec{v}_n(\omega) \quad ,$$

where ρ is the density of the helium film. This produces a force on the substrate equal to

$$\vec{F}(\omega) = i\omega A\,\vec{g}(\omega) = i\omega A\,[\rho - \rho_0/\epsilon(\omega)]\vec{v}_n(\omega) \quad .$$

Viewing the substrate as a simple harmonic oscillator of mass $M - \rho A$ and spring constant K we can write its equation of motion as

$$-\omega^2(M - \rho A)X(\omega) + KX(\omega)$$
$$= \omega^2 A[\rho - \rho_0/\epsilon(\omega)]X(\omega) \quad ,$$

where X is the displacement along $\vec{v}_n(\dot{X} = v_n)$.

Solving this gives a frequency of oscillation

$$\omega = \operatorname{Re}\left[\left[\frac{K}{M - A\rho_0/\epsilon(\omega)}\right]^{1/2}\right]$$

$$\simeq \left[\frac{K}{M}\right]^{1/2}\left[1 + \frac{A\rho_0}{2M}\operatorname{Re}[\epsilon^{-1}(\omega)]\right] \quad .$$

If we call $\omega_0 = \sqrt{K/M}$ then the period shift is

$$\frac{2\Delta P}{P} = 2\frac{\omega - \omega_0}{\omega_0} = \frac{A\rho_0}{M}\operatorname{Re}[\epsilon^{-1}(\omega)] \quad . \tag{A5}$$

We now discuss the numerical calculation of the dielectric constants. First we consider the contribution due to bound pairs.

To compute ϵ_b we need to calculate the static dielectric constant $\tilde{\epsilon}(r)$. In the notation of Kosterlitz and Nelson,[40]

$$\tilde{\epsilon}^{-1}(r) = \frac{K(l = \ln r/a)}{K(l = 0)} \quad , \qquad \text{(A6)}$$

where

$$K(0) = \frac{\hbar^2}{m^2} \frac{\rho_0}{k_B T} = \frac{2}{\pi} \frac{\rho_0 T_c}{\rho_s(T_c^-) T} \quad .$$

In the last equality, we have used the central result of the static scaling theory, described below, namely $\rho_s(T_c^-) = (2/\pi)m^2 k_B T_c/\hbar^2$. For the numerical fits it is convenient to express $K(0)$ in terms of $\rho_s(T_c^-)$. This permits the adjustment of the parameter $A\rho_s(T_c^-)/M$ to fit the experimental data, and thus a confrontation of theory and experiment, as described in the text.

K and the activity y satisfy the nonlinear scaling relations

$$\frac{dK^{-1}}{dl} = 4\pi^3 y^2, \quad \frac{dy^2}{dl} = 2(2 - \pi K)y^2 \quad . \qquad \text{(A7)}$$

If we introduce the parameter x related to K^{-1} by

$$K^{-1} = \frac{1}{2}\pi(1 - \frac{1}{2}x) \quad . \qquad \text{(A8)}$$

Then the scaling equations (A7) in terms of x and y become:

$$\frac{dx}{dl} = -(4\pi y)^2, \quad \frac{dy^2}{dl} = \frac{-2x}{1 - \frac{1}{2}x}y^2 \quad . \qquad \text{(A9)}$$

Using Eqs. (A3) and (A6)–(A9) we can write ϵ_b in terms of these variables as

$$\text{Re}(\epsilon_b) = \frac{\rho_0}{\rho_s(T_c^-)} \frac{T_c}{T}[1 - \frac{1}{2}x(l)] \quad ,$$
$$\qquad \text{(A10)}$$

$$\text{Im}(\epsilon_b) = \frac{1}{8}\pi \frac{\rho_0}{\rho_s(T_c^-)} \frac{T_c}{T}[4\pi y(l)]^2 \quad ,$$

evaluated at $l = \ln[(14D/a^2\omega)^{1/2}]$.

For small values of x and y the scaling Eq. (A9) may be linearized to give

$$\frac{dx}{dl} = -(4\pi y)^2, \quad \frac{dy^2}{dl} = -2xy^2 \quad . \qquad \text{(A11)}$$

These equations imply

$$x^2 - (4\pi y)^2 = -\frac{1}{4}b^2 t \quad , \qquad \text{(A12)}$$

where b is some constant and $t = 1 - T_c/T$, and thus the trajectories for small x and y are a set of hyperbolas. These are sketched in Fig. 14 with the arrows indicating the direction of increasing l. The solutions
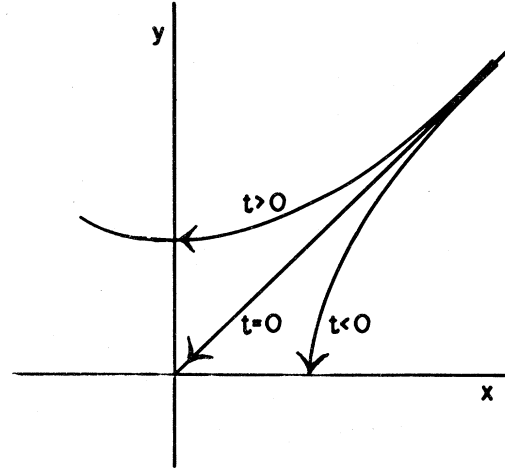

FIG. 14. Trajectories of Eq. (A12) for various values of t.

to the equations are

$$\left.\begin{array}{l} x(l) = x_0 \coth(x_0 l + \coth^{-1}x_i/x_0) \\ 4\pi y(l) = x_0 \operatorname{csch}(x_0 l + \coth^{-1}x_i/x_0) \end{array}\right\} \; t < 0 \; , \quad \text{(A13)}$$

$$\left.\begin{array}{l} x(l) = x_0 \cot(x_0 l + \cot^{-1}x_i/x_0) \\ 4\pi y(l) = x_0 \csc(x_0 l + \cot^{-1}x_i/x_0) \end{array}\right\} \; t > 0 \; , \quad \text{(A14)}$$

where $x_0 = \frac{1}{2}b|t|^{1/2}$ and $x_i = x(l = 0)$.

If we assume l is much larger than $1/x_i$ then we may drop the x_i dependent piece in Eqs. (A13) and (A14), which then reduce to

$$\left.\begin{array}{l} x(l) = x_0 \coth(x_0 l) \\ 4\pi y(l) = x_0 \operatorname{csch}(x_0 l) \end{array}\right\} \; t < 0 \; , \quad \text{(A15)}$$

$$\left.\begin{array}{l} x(l) = x_0 \cot(x_0 l) \\ 4\pi y(l) = x_0 \csc(x_0 l) \end{array}\right\} \; t > 0 \; . \quad \text{(A16)}$$

In these equations the information as to the starting point of the renormalization process has been lost.

If in the first formula of (A10) $[1 - \frac{1}{2}x(l)]$ is replaced by $[1 + \frac{1}{2}x(l)]^{-1}$ and the result is inserted into Eqs. (A4) and (A5) with x and y given by Eqs. (A15) and (A16), one obtains the "linear approximation" of Eqs. (11) and (12) of the main text. The replacement is of course only valid when $x(l) \ll 1$. However, the peak region of curves such as Fig. 10 corresponds to $x > 1$, with both x and y rapidly increasing on the high-temperature side of the peak. Thus the fits based on the linear approximation are somewhat spurious.

The precipitous drop at the high-temperature end of these curves is due in part to this approximation, and in part to the neglect of the free-vortex contribution (A2). In spite of these limitations, the "linear" fits have the advantage of being easy to use for ob-

taining values of $\rho_s(T_c^-)/T_c$ and b from experimental curves. The values so obtained differ only slightly from the results of the more elaborate fitting procedure we now describe.

The calculation referred to as "nonlinear" in the main text will now be described. [It should be emphasized that this calculation, leading to a response function $\epsilon(\omega)$, is still linear in the driving velocity v_n.]

Since for small $t < 0$, x and y remain small as l increases ($x \to x_0$, $y \to 0$), the linearized Eqs. (A15) are valid and were used in Eq. (A10) for determining ϵ_b for $T < T_c$. For $T > T_c$ however, x and y become large for large l and the linearized equations will breakdown. The procedure adopted for determining ϵ_b in this case is as follows.

In order to integrate out to a value l, the linearized Eqs. (A16) were used to go out an amount $l_0 = \pi/2x_0$ to the point $x(l_0) = 0$, $y(l_0) = (1/8\pi)b|t|^{1/2}$. The linearized equations are still good here as x and y have not yet grown large. Starting with this initial point $x(l_0), y(l_0)$ we then continue an additional amount $l - l_0$ by numerically integrating the nonlinear differential equations (A9). The values of $x(l)$ and $y(l)$ thus obtained are then used in Eqs. (A10) to determine ϵ_b.

Since the scaling Eqs. (A7) were derived only for the case $y \lesssim O(1)$, one cannot use the above procedure for T so large that $y(l = \ln(14D/a^2\omega)^{1/2}) > 1/4\pi$. Above the temperature T^* at which $y(l = \ln(14D/a^2\omega)^{1/2}) = 1/4\pi$, $\mathrm{Re}(\epsilon_b)$ was left at the value it had at T^*, and $\mathrm{Im}(\epsilon_b)$ was replaced by zero. The condition $y(l) \approx 1/4\pi$ is equivalent to the condition $l \approx \ln(\xi^+/a)$ where ξ^+ is the correlation length. Thus the modification has the physically sound interpretation of cutting off the contribution due to bound pairs when the separation, $\sqrt{14D/\omega}$, of those pairs which are most effective in the dynamical screening is equal to the average distance between vortices. Clearly, a pair of larger separation should actually be considered to be two free vortices. This discontinuous cut in ϵ_b has little effect on the shape of the Q^{-1} and $2\Delta P/P$ curves as ϵ_f is already dominating ϵ_b at these high temperatures. However, a small discontinuity is introduced into the calculated curves for $2\Delta P/P$ and Q^{-1}. This artificial discontinuity has been smoothed out in Fig. 12.

We now turn to the calculation of ϵ_f. The density of free vortices n_f can be related to the correlation length ξ^+ by

$$n_f = F/\xi^{+2} , \qquad (A17)$$

where F is some constant of $O(1)$. ξ^+ can be related to the parameter b introduced earlier by

$$\xi^+ = a \exp(2\pi/b\sqrt{t}) . \qquad (A18)$$

Combining these last two equations and substituting

them into Eq. (A2) gives

$$\epsilon_f = i\frac{F\rho_0 h^2}{14m^2kT}\frac{14D}{a^2\omega}\exp(-4\pi/b\sqrt{t})$$

$$= i\frac{4}{7}\pi F\frac{\rho_0 T_c}{\rho_s(T_c^-)T}\frac{14D}{a^2\omega}\exp(-4\pi/b\sqrt{t}) , \qquad (A19)$$

where, as in Eq. (A6), we have expressed the result in terms of $\rho_s(T_c^-)$. This completes the description of the method by which ϵ_b and ϵ_f are calculated. Note that the ρ_0 in Eqs. (A4) and (A5) for Q^{-1} and $2\Delta P/P$ cancels the ρ_0 in Eqs. (A10) and (A19) for ϵ_b and ϵ_f. Also, for the range of temperatures being considered, $T_c/T \simeq 1$ in Eqs. (A10) and (A19). Thus the free parameters of the theory are $\rho_s(T_c^-)A/M$, b, $14D/a^2\omega$, F, and T_c.

In order to fit the experimentally observed low-temperature background dissipation, an additional fixed constant ϵ' was added to the imaginary part of $\epsilon(\omega)$. Using $\epsilon(\omega) = i\epsilon' + \epsilon_b + \epsilon_f$ in Eqs. (A3) and (A4), curves were generated for Q^{-1} and $2\Delta P/P$. These curves were then fitted to the data by varying the six free parameters. The values obtained for the fitted curve shown are (Fig. 12).

$$\rho_s(T_c^-)A/M = 3.4 \times 10^{-6} , \quad b = 5.5 ,$$

$$\ln[(14D/a^2\omega)^{1/2}] = 12 , \quad F = 1.2 ,$$

$$T_c = 1.2043 , \quad \epsilon' = 0.07 .$$

It should be pointed out that these fitted parameters should apply for a wide range of frequencies if the basic ideas of the theory are correct. (The parameter ϵ', whose physical origin has not been clarified may have a frequency dependence, but ϵ' contributes little to $\Delta P/P$ and Q^{-1} in the interesting $T > T_c$ region.) It may also be worth noting that the value of the dynamical parameter $\ln[(14D/a^2\omega)^{1/2}]$ is not inconsistent with D being related to microscopic quantities, $D \sim \hbar/m$, and $a \sim 10^{-8}$ cm.

APPENDIX B

To derive formulas (8) and (9), we first start with

$$T_c = A(\rho - \rho_0) , \qquad (B1)$$

$$\rho_s(0) = (1-\chi)(\rho - \rho_0) , \qquad (B2)$$

where $(1-\chi)$ is the fraction of a superfluid helium which is able to superflow at $T = 0$. χ is the fraction of superfluid which remains effectively locked to the substrate by its inertia:

$$\rho_s(T) = \rho_s(T_c^-)[1 + b(1 - T/T_c)^{1/2}] , \qquad (B3)$$

$$\rho_s(T_c) = (1-\chi)CT_c , \qquad (B4)$$

where C is the Kosterlitz-Thouless static value of $8.75\ \mu\text{mol}/\text{m}^2\text{K}$. Taking Eq. (B3) and setting $T = 0$ we obtain

$$\rho_s(0) = \rho_s(T_c^-)(1 + b)\ .\tag{B5}$$

Using Eq. (B2) we obtain

$$(1 - \chi)(\rho - \rho_0) = \rho_s(T_c^-)(1 + b)\ ,\tag{B6}$$

with Eq. (B1) this becomes

$$(1 - \chi)T_c/A = \rho_s(T_c^-)(1 + b)\ .\tag{B7}$$

Using Eq. (B4) we obtain

$$(1 - \chi)T_c/A = (1 - \chi)CT_c(1 + b)$$

or

$$b = (1/AC - 1)\ .\tag{B8}$$

Using Eqs. (B8), (B1), and (B4) we see that Eq. (B3) becomes

$$\rho_s(T) = (1 - \chi)AC(\rho - \rho_0)$$
$$\times\left[1 + \left(\frac{1}{AC} - 1\right)\left(\frac{T_c - T}{T_c}\right)^{1/2}\right]\ .\tag{B9}$$

The jump occurs at $\rho = \rho_1$, $T = T_1$. Using Eq. (B1) we find

$$T_1 = A(\rho_1 - \rho_0)\ .\tag{B10}$$

Therefore using Eqs. (B10) and (B1), Eq. (B9) becomes

$$\rho_s(T) = (1 - \chi)AC(\rho - \rho_0)$$
$$\times\left[1 + \left(\frac{1}{AC} - 1\right)\left(\frac{\rho - \rho_1}{\rho - \rho_0}\right)^{1/2}\right]\ .\tag{B11}$$

The final result is now at hand. For $\rho < \rho_1$ we find that

$$\tau = \left(\frac{\Delta P}{\Delta \rho}\right)\rho + P_0\ ,\tag{B12}$$

where $(\Delta P/\Delta \rho)$ and P_0 are the slope and intercept of the normal-fluid region in Fig. 9. For $\rho > \rho_1$ we find that

$$\tau = \left(\frac{\Delta P}{\Delta \rho}\right)\rho + P_0 - \left(\frac{\Delta P}{\Delta \rho}\right)(1 - \chi)AC(\rho - \rho_0)$$
$$\times\left[1 + \left(\frac{1}{AC} - 1\right)\left(\frac{\rho - \rho_1}{\rho - \rho_0}\right)^{1/2}\right]\ ,\tag{B13}$$

where A is the slope of the transition temperature versus density line. It is $0.086\,96\ \text{K m}^2/\mu\text{mol}$; C is the Kosterlitz-Thouless jump and is given by $8.75\ \mu\text{mol}/\text{m}^2\text{K}$; ρ is the density of adsorbed film; ρ_0 is the solid layer density, given by $24.91\ \mu\text{mol}/\text{m}^2$; and χ is the fraction of superfluid coupled to the sur-

face. Therefore Eqs. (B12) and (B13) describe the experiment in Fig. 9 with one adjustable parameter χ.

APPENDIX C

For a summary of the data see Table I.

TABLE I. Summary of data.

	T_c (K)	$\rho_s(T_c)/\rho$ (10^9 g/cm^2)
Bishop and Reppy, T_c = const	0.330	0.860
	0.353	1.117
	0.355	1.427
	0.390	1.535
	0.470	1.546
	0.498	1.803
	0.522	1.710
	0.540	1.424
	0.543	2.013
	0.588	1.867
	0.587	1.875
	0.590	1.801
	0.593	1.783
	0.698	2.607
	0.835	2.703
	0.882	3.794
	0.886	3.108
	0.896	3.429
	0.908	3.105
	0.909	3.026
	0.909	2.934
	0.908	2.945
	0.911	2.698
	0.914	2.807
	1.079	4.418
	1.088	4.123
	1.090	3.958
	1.092	3.954
	1.093	3.961
	1.094	3.986
	1.189	4.294
	1.192	4.400
	1.600	5.040
Bishop and Reppy, T = const	0.350	1.23
	0.312	1.42
	0.520	2.73
	1.230	4.97
Hallock, 3rd sound	1.721	6.32
	1.675	5.80
Mochel, 3rd sound	0.460	1.10
	0.681	2.42
	0.972	3.44
	1.040	3.66
	1.160	4.39
	1.330	4.82

*Present address: Bell Laboratories, Murray Hill, N. J. 07974.

[1]D. J. Bishop and J. D. Reppy, Bull. Am. Phys. Soc. 22, 638 (1977); 23, 532 (1978).

[2]D. J. Bishop and J. D. Reppy, Phys. Rev. Lett. 40, 1727 (1978).

[3]D. J. Bishop and J. D. Reppy, J. Phys. (Paris) 39, C6-339 (1978).

[4]B. A. Huberman, R. J. Myerson, and S. Doniach, Phys. Rev. Lett. 40, 780 (1978).

[5]V. Ambegaokar, B. I. Halperin, D. R. Nelson, and E. D. Siggia, Phys. Rev. Lett. 40, 783 (1978).

[6]F. Bloch, Z. Phys. 61, 206 (1930).

[7]R. Peierls, Ann. Inst. Henri Poincare 5, 177 (1935).

[8]M. F. M. Osborne, Phys. Rev. 76, 396 (1949).

[9]N. D. Mermin, Phys. Rev. 176, 250 (1968).

[10]N. D. Mermin and H. Wagner, Phys. Rev. Lett. 22, 1133 (1966).

[11]P. C. Hohenberg, Phys. Rev. 158, 383 (1967).

[12]B. V. Rollin, Actes du 7e Congr. Intern du Froid (La Haye: Amsterdam), 1, 187 (1936).

[13]J. G. Daunt and K. Mendelssohn, Proc. R. Soc. London, Sect. A 170, 423, 439 (1939).

[14]E. Long and L. Meyer, Phys. Rev. 79, 1031 (1950); 85, 1030 (1952).

[15]R. Bowers, D. F. Brewer, and K. Mendelssohn, Philos. Mag. 42, 1445 (1951).

[16]E. N. Smith, D. J. Bishop, J. E. Berthold, and J. D. Reppy, in Ref. 3.

[17]See, for example, J. G. Dash, Films on Solid Surfaces (Academic, New York, 1975); Phys. Lett. C 38, 177 (1978); D. F. Brewer, in The Physics of Liquid and Solid Helium, edited by K. H. Benneman and J. B. Ketterson (Wiley, New York, 1978); J. M. Kosterlitz and D. J. Thouless, in Progress in Low Temperature Physics, edited by D. F. Brewer (North-Holland, Amsterdam, 1978), Vol. VII b.

[18]J. M. Ziman, Philos. Mag. 44, 548 (1953).

[19]D. L. Mills, Phys. Rev. 134, A306 (1964).

[20]B. M. Khorana and D. H. Douglass, Phys. Rev. 138, A35 (1965).

[21]D. F. Goble and L. E. H. Trainor, Phys. Lett. 18, 122 (1965); Can. J. Phys. 44, 27 (1966); Phys. Rev. 157, 167 (1967).

[22]R. L. Dewar and N. E. Frankel, Phys. Rev. 165, 283 (1968).

[23]O. Penrose—a paper presented at the conference in honor of Professor Lars Onsager's 70th birthday held at University of Miami, Nov. 27–28, 1973 (unpublished).

[24]G. Lasher, Phys. Rev. 172, 224 (1968).

[25]V. L. Berezinskii, Sov. Phys. JETP 32, 493 (1970); 34, 610 (1971).

[26]J. M. Kosterlitz and D. J. Thouless, J. Phys. C 5, L124 (1972); 6, 1181 (1973).

[27]O. Penrose and L. Onsager, Phys. Rev. 104, 576 (1956).

[28]I. Rudnick, R. S. Kagiwada, J. C. Fraser, and E. Guyon, Phys. Rev. Lett. 20, 430 (1968).

[29]H. P. Henkel, G. Kukich, and J. D. Reppy, in Proceedings of 11th International Conference on Low Temperature Physics, St. Andrews, U. K., 1968, edited by J. F. Allen, D. M. Finlayson, and D. M. McCall (St. Andrews University Press, St. Andrews, Scotland, 1969).

[30]S. J. Putterman, R. Finkelstein, and I. Rudnick, Phys. Rev. Lett. 27, 1697 (1971).

[31]M. Chester and L. C. Yang, Phys. Rev. Lett. 31, 1377 (1973).

[32]J. A. Herb and J. G. Dash, Phys. Rev. Lett. 29, 846 (1972).

[33]E. L. Andronikashvili, Zh. Eksp. Teor. Fiz. 16, 780 (1946).

[34]J. E. Berthold, D. J. Bishop, and J. D. Reppy, Phys. Rev. Lett. 39, 348 (1977).

[35]D. J. Bishop, J. E. Berthold, J. M. Parpia, and J. D. Reppy (unpublished).

[36]See D. J. Bishop, Ph.D. thesis (Cornell University, 1978) (unpublished).

[37]E. D. Siggia (private communication).

[38]J. M. Kosterlitz, J. Phys. C 7, 1046 (1974).

[39]J. V. Jose, L. P. Kadanoff, S. Kirkpatrick, and D. R. Nelson, Phys. Rev. B 16, 1217 (1977).

[40]D. R. Nelson and J. M. Kosterlitz, Phys. Rev. Lett. 39, 1201 (1977).

[41]See for example P. R. Bevington, Data Reduction and Error Analysis for the Physical Sciences (McGraw-Hill, New York, 1969).

[42]I. Rudnick, Phys. Rev. Lett. 40, 1454 (1978).

[43]J. Mochel (private communication); R. Hallock (private communication).

[44]J. A. Roth, G. J. Jelatis, and J. D. Maynard, Phys. Rev. Lett. 44, 333 (1980).

[45]Mylar is a trade name registered to the E. I. Dupont de Nemours Company, Inc.

[46]E. Webster, G. Webster, and M. Chester, Phys. Rev. Lett. 42, 243 (1979).

[47]V. Ambegaokar and S. Teitel, Phys. Rev. B 19, 1667 (1979).